

SEVENTEENTH EUROPEAN ROTORCRAFT FORUM

Paper No. 91 - 63

SOUND PRODUCED BY VORTEX-AIRFOIL INTERACTION

K. EHRENFRIED¹⁾, G.E.A. MEIER²⁾, F. OBERMEIER³⁾

1).3) MAX-PLANCK-INSTITUT f. STRÖMUNGSFORSCHUNG, GÖTTINGEN, GERMANY

2) DLR-INSTITUT f. EXPERIMENTELLE STRÖMUNGSMECHANIK, GÖTTINGEN, GERMANY

SEPTEMBER 24 - 26, 1991

Berlin, Germany

Deutsche Gesellschaft für Luft- und Raumfahrt e.V. (DGLR)

Godesberger Allee 70, 5300 Bonn 2, Germany

OPGENOMEN IN
GEAUTOMATISEERDE
CATALOGUS

N 61332



Sound Produced by Vortex-Airfoil Interaction

K. Ehrenfried¹⁾, G.E.A. Meier²⁾, F. Obermeier³⁾

1).3) Max-Planck-Institut f. Strömungsforschung, Göttingen, Germany

2) DLR-Institut f. Experimentelle Strömungsmechanik, Göttingen, Germany

Abstract

Transonic vortex-airfoil interactions are numerically investigated. The numerical calculations are done by solving the unsteady two-dimensional Euler equations on an unstructured grid surrounding a NACA0012 airfoil. The simulations show that several mechanisms of sound generation are effective during the vortex-airfoil interaction. From the numerical results an overview of the processes which occur is given. Additionally the numerical results are compared with experiments and the influence of the Mach number and other parameters on the sound production is discussed.

Introduction

The two-dimensional vortex-airfoil interaction is investigated as a model for the three-dimensional process where the tip vortex of a helicopter rotor blade interacts with a following blade. Of most interest is the case where a single vortex passes an airfoil and the vortex rotates in the direction so that the flow around the airfoil is accelerated at the beginning of the interaction. This two-dimensional model contains all significant features of the sound production during the three-dimensional interaction. Experimental studies (Ref. 1 to 3) of the two-dimensional case show two major mechanisms which cause impulsive sound waves. These experiments were done in a shock tube (Ref. 3) and a wind tunnel (Ref. 1 and 2) using Mach-Zehnder interferometry to obtain the density distribution in the flow field. But only the density distribution is not sufficient to understand the mechanisms of sound generation in detail. A density variation in the flow field may be combined with a pressure or an entropy variation. It is therefore impossible to calculate the circulation of a vortex from the density distribution alone. For instance a vortex with a relatively hot core and a weak radial pressure gradient might have the same density field as an adiabatic vortex with a stronger, radial pressure gradient.

In addition to the density other quantities like the flow velocity or the pressure are very difficult to measure. To obtain information on the temperature or the entropy distribution in the flow field, density and pressure must be evaluated simultaneously. Mandella and Bershader (Ref. 4) show some results produced in this manner. Among other things they calculated the temperature in a compressible vortex using locally measured pressure data.

This method is therefore limited to the position where the pressure gauge is located. If more pressure gauges are used, the optical measurement of the density is hindered. Thus it is technically difficult to obtain both the complete density and pressure field at the same time.

In contrast to the experiment, numerical calculations yield the full information on the flow field. Interesting quantities like the temperature, pressure or vorticity are determined by the numerical solution. This may help to understand the mechanisms of sound generation. Examples of numerical simulations dealing with the vortex-airfoil interaction can be found in Ref. 5 to 8. But numerical calculations also involve difficulties. The common numerical problem is the accuracy of the solution with regard to artificial viscosity and other discretisation effects. Thus the verification of the numerical solutions by experiments is imperative. In order to compare numerical and experimental results directly, the same boundary and initial conditions have to be used in both cases. As mentioned above only the experimental density distribution is known. But for the numerical calculation also the initial value of the other quantities apart from the density are required. Thus some assumptions are made to start the calculation. The density distribution of the initial vortex is chosen close to the one of a typical experimental vortex. Because of the lack of other information simply homentropic state is assumed in the vortex. Due to the given density distribution the vortex is of finite size. This is different from the mentioned calculations in Ref. 5 to 8 where vortices of Lamb-Oseen type are used. One advantage of the finite size is that the vortex fits completely inside the computational domain and no boundary condition is violated by inserting it.

Beside the assumption on the vortex the second problem is in which solution this vortex should actually be inserted. Here a steady solution is used like in the cited references. But in the experimental studies the flow field around the airfoil seems to be only partially similar to the steady solution. In shock tube experiments (Ref. 3) the flow around the airfoil is accelerated by a shock wave. The vortex is generated upstream of the airfoil by this shock wave. Typically the time between the beginning of the acceleration of the flow around the airfoil and the arriving of the vortex in this region is relatively short. Thus the flow field around the airfoil is not developed to the steady flow at the beginning of the interaction. A similar situation can be found in the wind tunnel experiments (Ref. 1 and 2) where upstream of the airfoil a permanent Karman vortex street is generated and the interaction of the vortices is observed. Thus the airfoil interacts with a complete Karman vortex street rather than a single vortex. The time between two interactions is much too short to adapt a steady solution.

Although these facts lead to different initial conditions between the numerical and the experimental case the investigations in this paper will show that mostly a qualitatively good correspondence between numerical and experimental results can be observed. The advantage is that by the numerical calculations, where the initial condition is exactly known

and the full information about the flow field is available, the vortex-airfoil interaction can be investigated in a more specific way. Of course there are an infinite number of possible boundary conditions. Thus we restrict ourself to a few examples which are typical and important for the helicopter problem.

Numerical Procedure

The numerical calculations are done by the solution of the unsteady, two-dimensional Euler equations

$$\frac{\partial}{\partial t}q + \frac{\partial}{\partial x}f(q) + \frac{\partial}{\partial y}g(q) = 0 \quad . \quad (1)$$

The state vector q and the fluxes f and g in x and y direction respectively are given by

$$q = \begin{pmatrix} \rho \\ \rho u \\ \rho v \\ \rho e \end{pmatrix}, \quad f = \begin{pmatrix} \rho u \\ \rho u^2 + p \\ \rho uv \\ u(\rho e + p) \end{pmatrix} \quad \text{and} \quad g = \begin{pmatrix} \rho v \\ \rho uv \\ \rho v^2 + p \\ v(\rho e + p) \end{pmatrix} \quad (2)$$

where ρ denotes density, p pressure, u and v the velocity components in x and y direction and e the specific total energy. This set of equations is completed with the equation of state for ideal gas

$$p = (\gamma - 1) \rho \left(e - \frac{1}{2}(u^2 + v^2) \right) \quad (3)$$

where γ represents the ratio of specific heats. The calculation is done on an unstructured grid around a NACA0012 airfoil. The grid which consists of triangles is shown in Fig. 1. The upper and lower side of the computational domain are treated as rigid walls like the surface of the airfoil. On the left side quasisteady inflow conditions are used where constant entropy, constant stagnation enthalpy and parallel flow is given. On the right side of the computational domain an outflow condition with constant pressure is applied.

An implicit finite-volume-scheme with second order temporal accuracy is used. The finite volumes are two-dimensional cells which were constructed in the triangles of the grid. The essential features of this method can be found in Ref. 9. The numerical flux at the boundaries of the cells is calculated by flux-difference-splitting where Oshers approximative Rieman solver is used. A special technique is applied for the interpolation of the quantities at the cell boundaries. Depending on the smoothness of the solution this method switches continously from upwind to central discretisation. This way the captured shock waves are sharp and produce no unphysical ocllations and at the same time the numerical dissipation is reduced drastically compared to usual low order schemes. A detailed description of the whole method is given in Ref. 10. In the following all quantities are normalized by the cord lenght L_c and the velocity $v_0 = (p_0/\rho_0)^{1/2}$ where p_0 and ρ_0 are the stagnation values of pressure and density.

Initial condition

The calculation starts with a steady solution $q_{steady}(x, y)$ into which a vortex is inserted. A typical density field at the beginning of the calculation is shown in Fig. 2. The vortex is inserted in a region far away from the airfoil where the disturbance of the parallel flow by the airfoil is negligible. For the calculation of the quantities in the vortex the assumption is made that the vortex is in exact parallel flow (indicated by the index ||). The density distribution $\rho_w(r)$ in the vortex is given by

$$\rho_w(r) = \begin{cases} \rho_{||} - \Delta\rho_w \frac{1}{2} \left[1 + \sin \left(\pi \left(\frac{R-r}{R} \right)^3 - \frac{\pi}{2} \right) \right] & \text{if } 0 \leq r \leq R \\ \rho_{||} & \text{if } r > R \end{cases} \quad (4)$$

where r denotes the radius. The parameters $\Delta\rho_w$ and R determine the form of the vortex. $\Delta\rho_w$ is the density decline in the center of the vortex and R is the radial extent of the vortex. In all cases which will be presented here these values are kept fixed to: $\Delta\rho_w = 0.25$ and $R = 1.0$. Together with the radial momentum equation

$$\frac{\partial p_w}{\partial r} = \rho_w \frac{v_\theta^2}{r} \quad (5)$$

and the assumptions of ideal gas and constant entropy in the vortex the state $q_w(x, y)$ inside the vortex is determined. Thereby v_θ denotes the tangential velocity in the vortex. Due to the finite size of the vortex the circulation $\Gamma(r) = 2\pi r v_\theta(r)$ has a maximum for a certain radius and vanishes smoothly for $r \rightarrow R$. This is different from the usually used vortices of Lamb-Oseen type where $\Gamma(r)$ increases monotonously to a finite value for $r \rightarrow \infty$. In our case the maximum circulation Γ_{max} is a good measure for the strength of the vortex.

The insertion of the vortex is done in a special manner. The initial solution is given by

$$q_{ini}(x, y) = \begin{cases} q_{steady}(x, y) - q_{||} + q_w(x, y) & \text{if } 0 \leq r \leq R \\ q_{steady}(x, y) & \text{if } r > R \end{cases} \quad (6)$$

where r is the distance from the center (x_0, y_0) of the vortex:

$$r = \sqrt{(x - x_0)^2 + (y - y_0)^2} \quad (7)$$

Before $q_w(x, y)$ and $q_{ini}(x, y)$ can be calculated the state $q_{||}$ has to be specified. Here simply the steady state in the point (x_0, y_0) is taken as the hypothetical parallel flow for which the vortex is calculated: $q_{||} = q_{steady}(x_0, y_0)$.

This special procedure guarantees that the initial solution $q_{ini}(x, y)$ has no discontinuities. Thus the inserted vortex causes no disturbances at the beginning of the calculation.

It is simply convected in the flow until the interaction with the airfoil starts. Of course this requires that the vortex is inserted in a region where the steady solution $q_{steady}(\mathbf{x}, \mathbf{y})$ is nearly constant and no boundary conditions are violated. This means that the vortex must fit completely inside the computational domain. The initial solution shown in Fig. 2 fulfils these conditions and the following results will show that no disturbances occur at the beginning of the calculation due to the insertion of the vortex.

Numerical results

Before the details of the sound generation mechanisms are investigated in the following a global overview of the vortex-airfoil interaction is given. A typical example is chosen therefore where the initial position of the vortex is $(x_0, y_0) = (-2.0, -0.25)$. The free stream pressure is $p_{||} = 0.8$ corresponding to a Mach number of $Ma \approx 0.57$. For that case the initial solution at $t = 0$ was already shown in Fig. 2. The dimensionless circulation of the vortex is $\bar{\Gamma}_{max} = \Gamma_{max} / (L_c u_{||}) = 1.56$. In Fig. 3 the pressure distributions at three following moments are depicted. At $t = 2.4$ the vortex approaches the airfoil and the interaction begins. The stagnation point is shifted towards the upper surface of the airfoil. At $t = 3.6$ the vortex is right under the airfoil. A shock wave is present between the airfoil and the core of the vortex. The reason for this is that the vortex accelerates the flow near the airfoil and generates a region of supersonic flow. This region is terminated by the shock wave. The whole configuration moves downstream as the vortex is convected. At this time already various waves were generated by the interaction. Most significant is the compression wave which is in front of the airfoil. The motion of the stagnation point, which moved back in the meantime and has reached the lower surface of the airfoil, is correlated with a temporal increase of the stagnation pressure. The unsteady pressure distribution at the surface of the airfoil produces the mentioned compression wave. This wave is called *compressibility wave* in the following. The shape of the wave front indicates that the origin of the wave is a small region close to the nose of the airfoil.

Before the *compressibility wave* is generated a rarefaction wave propagates from the lower side of the airfoil towards the lower limitation of the computational domain. At $t = 3.6$ this wave has reached the lower channel wall and the pressure is decreased there. Later at $t = 4.8$ the *compressibility wave* has also reached the lower channel wall and the pressure there is increased again. At this time already several reflections can be observed at the channel walls. Especially in the region close to the upper channel wall the flow field is influenced by a reflected wave. At this wall the *compressibility wave* has arrived earlier than at the lower wall.

The solution becomes more complicated due to the reflections. But in the region around the airfoil the flow is still not affected by the reflections. The vortex is downstream of the trailing edge of the airfoil at $t = 4.8$. The supersonic region which is generated by

the vortex at the lower side of the airfoil collapses when the vortex moves away from the airfoil. Then the shock wave which terminates the supersonic region becomes weaker and it starts to travel upstream. In Fig. 3c the remainder of the shock wave is visible as a second compression wave which has just reached the leading edge of the airfoil. This wave is called *transonic wave*. The situation at $t = 4.8$ becomes more clear in Fig. 4 where the pressure is plotted in a quasi-three-dimensional way. The airfoil is raised in this picture to mark its position. The vortex is visible as a pressure minimum and both the compression waves and their reflections appear clearly.

Comparison with experiments

In the example which was presented in the last section several sound generation mechanisms are effective. The occurrence of each mechanism depends on many parameters as the Mach number, the vortex structure, the vortex strength and the initial position (x_0, y_0) . The major effects are the two impulsive waves which are generated. In the presented example the parameters were chosen so that both waves appear. But in many cases only one of the mechanisms is effective. The *compressibility wave* is caused by the unsteady pressure variations on the airfoil surface in the nose region. These variations depend on the velocity which is induced by the vortex in this region. As experimentally shown in Ref. 3 the exact geometry of the airfoil is not significant for the sound production. Also at blunt bodies or cylinders the impulsive *compressibility wave* is always generated when a vortex interacts with them. The wave occurs if the vortex passes the body sufficiently close and if it is strong enough to produce a visible effect. For weaker vortices the *compressibility wave* may play a minor role and the *transonic wave* dominates the process. One experimental example for that case is shown in Fig. 5 which is taken from Ref. 11. The experiment was done in a wind tunnel at Mach number $Ma = 0.6$ and the airfoil is an OLS profile. The time step between the interferograms is 0.2msec . The velocity which is induced by the vortex at the nose of the airfoil is too weak to produce a visible *compressibility wave*. But the vortex generates a supersonic flow region at the lower side of the airfoil like the vortex in the numerical example in Fig. 3. The last interferogram shows the *transonic wave* in a position further upstream. Due to the diffraction at the nose of the airfoil the form of the wave front is similar to the one of the *compressibility wave* in the numerical example. So there are two mechanisms to generate impulsive waves which seem to have their origin at the leading edge of the airfoil.

In Ref. 1 the parameter range of the Mach number and the vortex circulation in which the transonic wave occurs were determined experimentally. In this work the circulation was calculated by the assumption of an isentropic flow field. The difficulties involved with that method were already discussed above. However, also relatively weak vortices which have low circulation may generate a transonic wave. This depends on the Mach number. If the Mach number is too low a weak vortex is not able to generate a supersonic region at the airfoil. If

the Mach number is too high supersonic regions with steady shock waves are already present at the airfoil. In this case a weak vortex only disturbs the steady configuration. The shock waves stay at the airfoil and no transonic wave is generated. This case was already calculated numerically in Ref. 6 and 7. Only in a certain range between these limits a weak vortex generates the transonic wave. In contrast to the production of the *compressibility wave* also the geometry of the airfoil is important for the generation of the *transonic wave*, because the geometry determines the Mach number range in which the conditions are given for the generation of the supersonic region.

Additional effects

Beside the discussed two mechanisms of impulsive noise generation during the interaction additional effects may occur where shock waves and noise is produced. In the following the case is regarded where the channel pressure is $p_{||} = 0.7$ and all other parameters are the same as in the example shown in Fig. 3. Due to the higher channel velocity $u_{||}$ the dimensionless circulation of the vortex is now $\bar{\Gamma}_{max} = 1.28$. The pressure $p_{||} = 0.7$ corresponds to a Mach number of $Ma \approx 0.73$. This Mach number is close to the value where the steady flow becomes transonic. But in the regarded case no shocks are present in the initial solution. In Fig. 6a the pressure distribution at $t = 4.0$ is plotted for a sector around the airfoil. At this time the vortex has already passed the airfoil and it's position is nearly the same as the position of the vortex in Fig. 3c for the lower Mach number. In contrast to the case with lower Mach number also a shock wave is present at the upper side of the airfoil. This shock limits a supersonic region which is generated by the vortex additionally to the one on the lower side of the airfoil. Close to the trailing edge a second compression wave which travels upstream can be seen on the upper side of the airfoil. Such a wave can also be found in the case of the lower Mach number. These waves are caused by waves which travel downstream along the airfoil and are reflected and diffracted at the trailing edge. These downstream travelling waves are generated by the vortex when it is leaving the airfoil and the shock wave below the airfoil is released.

These effects can also be found in experiments. In Fig. 6b, which is taken from Ref. 12, an example is shown. The interferogram shows the density distribution after the interaction of a vortex with the NACA0012 profile. The vortex position is close to that in the numerical example. In the experiment the Mach number was $Ma = 0.8$. This is higher than in the numerical example and the experiment was done in a wind tunnel using vortices of a Karman vortex street. It was already discussed in the introduction that such experiments are not directly comparable to the numerical calculations which start with a steady flow around the airfoil. But the additional effect of the shock wave on the upper surface occurs also in the experiment. And similar to the calculation the additional wave close to the trailing edge is present too. From the calculations one can estimate that the generation of the waves on

the upper side is not influenced by reflections from the side walls of the channel. In the numerical example both waves travel in upstream direction and meet at $t \approx 6.0$. These waves are an additional source of noise which is radiated from the region around the airfoil.

Conclusions

The numerical calculations show that several mechanisms of sound generation are effective during the vortex-airfoil interaction. The generation of the *compressibility wave* and the *transonic wave* are the major processes which are responsible for the impulsive noise. The calculations proofed that several effects which were already observed in experiments are produced by the vortex-airfoil interaction and not by side effects like reflection from channel walls. In many experiments a Karman vortex street is used to investigate the vortex-airfoil interaction. The calculation shows that in spite of disturbances of the flow by previous vortices of the street and the influences of the vortices on each other these experiments model the case of a single vortex in a good manner. Using the same geometry with side walls as in the typical experiments the calculations show how far the reflections from the walls influence the interaction process at a given time. This helps to interpret experimental results where the flow is observed only in a restricted part of the channel.

The results presented here are also important for the helicopter problem. One major intention is the reduction of noise generated by helicopters. The presented results show that the designers have to take into account that already in the two-dimensional model different mechanisms of sound generation are effective. In reality additional three-dimensional effects may be involved. The reduction of one effect may amplify the other sound generation processes. Thus all different phenomena have to be regarded.

References

1. G.E.A. Meier, U. Schievelbusch and H.-M. Lent, Stoßwellenentstehung bei transsonischer Wirbel-Profil-Wechselwirkung, **Z. Flugwiss. Weltraumforsch.**, Vol. 14 (1990), pp. 327-332.
2. G.E.A. Meier and R. Timm, Unsteady Vortex Airfoil Interaction, **AGARD Conf. Proc.**, Vol. 386, AGARD, Neuilly sur Seine 1985, 16:1-10 (1985).
3. H.-M. Lent, Modell für die Schallentstehung bei kompressibler Wirbel-Körper-Wechselwirkung, **Mitteilungen aus dem MPI f. Strömungsforschung**, Nr. 96 (1990).
4. M. Mandella and D. Bershader, Quantitative Study of the Compressible Vortex: Generation, Structure and Interaction with Airfoils, **AIAA Paper 87-0328**, AIAA 25th Aerospace Sciences Meeting, Reno, Nevada, January 1987.

5. C.S. Kocaaydin, Aerodynamik der Impulsschallentstehung durch Wirbel-Profil-Wechselwirkung, **VDI Fortschrittberichte**, Reihe 7: Strömungstechnik, Nr. 180 (1990).
6. M.M. Rai, Navier-Stokes Simulations of Blade-Vortex Interaction Using High-Order Accurate Upwind Schemes, **AIAA-Paper 87-0543**, AIAA 25th Aerospace Sciences Meeting, Reno, Nevada, January 1987.
7. G.R. Srinivasan, W.J. McCroskey and J.D. Baeder, Aerodynamik of Two-Dimensional Blade-Vortex Interaction, **AIAA Journal**, Vol. 24, No. 10 (1986), pp. 1569-1576.
8. N.-S. Liu, F. Davoudzadeh, W.R. Briley and S.J. Shamroth, Navier-Stokes Simulation of Transonic Blade-Vortex Interactions, **J. Fluids Engineering**, Vol. 112 (1990), pp. 501-509.
9. G. Vijayasundaram, Transonic Flow Simulations Using an Upstream Centered Scheme of Godunov in Finite Elements, **J. Comp. Phy.**, Vol. 63 (1986), pp. 416-433.
10. K. Ehrenfried, Numerische Untersuchung von Wirbel-Tragflügel-Wechselwirkungen im transsonischen Geschwindigkeitsbereich, Doctoral Thesis, Universität Göttingen (1991).
11. K. Löhr, Zur Aeroakustik der Wechselwirkung von Wirbeln mit transsonisch umströmten Körpern, **Max-Planck-Institut f. Strömungsforschung**, Report No. 3/1988 (1988).
12. K.J. Müller, Einfluß der Kompressibilität auf die Kutta-Bedingung, Diploma Thesis, Göttingen (1990).

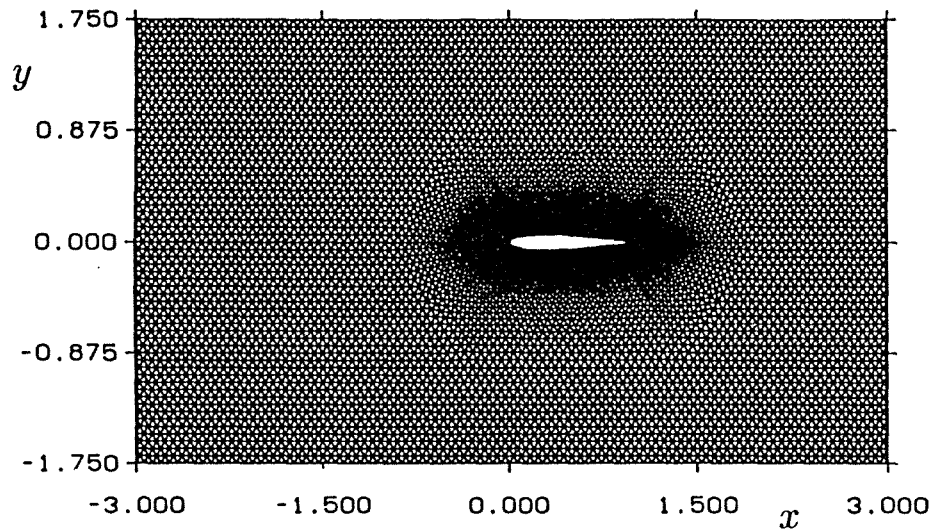


Fig. 1: Unstructured grid around NACA0012 airfoil

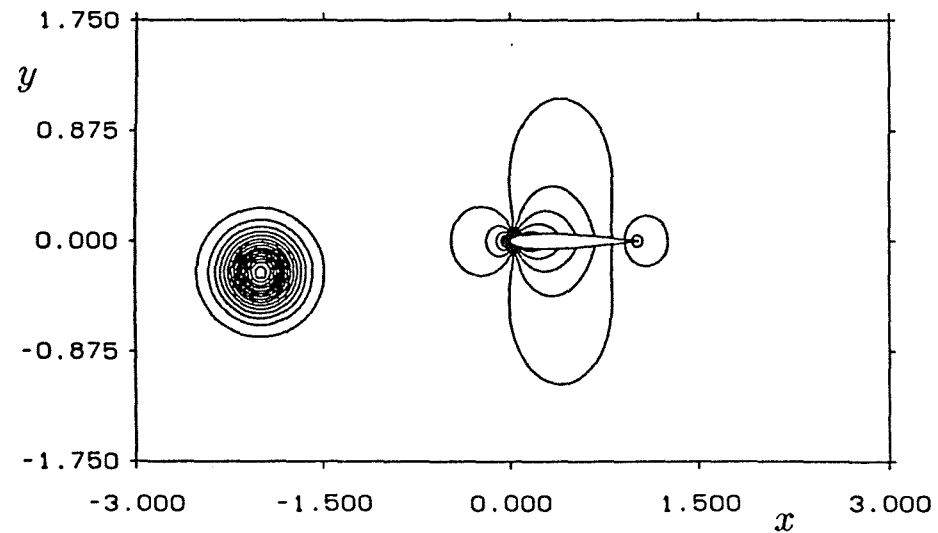


Fig. 2: Typical initial pressure distribution;
 $Ma \approx 0.57, \bar{\Gamma}_{max} = 1.56, y_0 = -0.25$

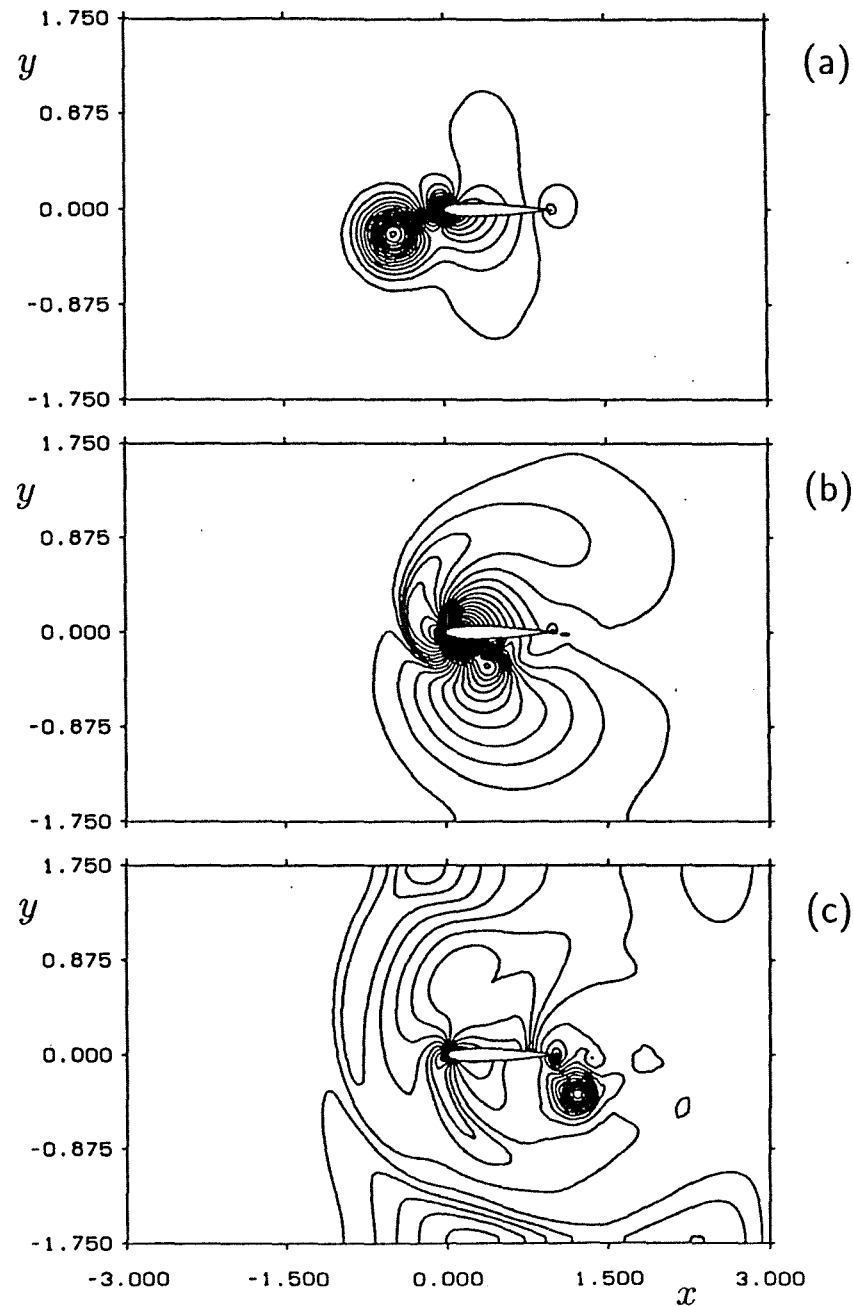


Fig. 3: Pressure distribution at (a) $t = 2.4$, (b) $t = 3.6$ and (c) $t = 4.8$;
 $Ma \approx 0.57, \bar{\Gamma}_{max} = 1.56, y_0 = -0.25$

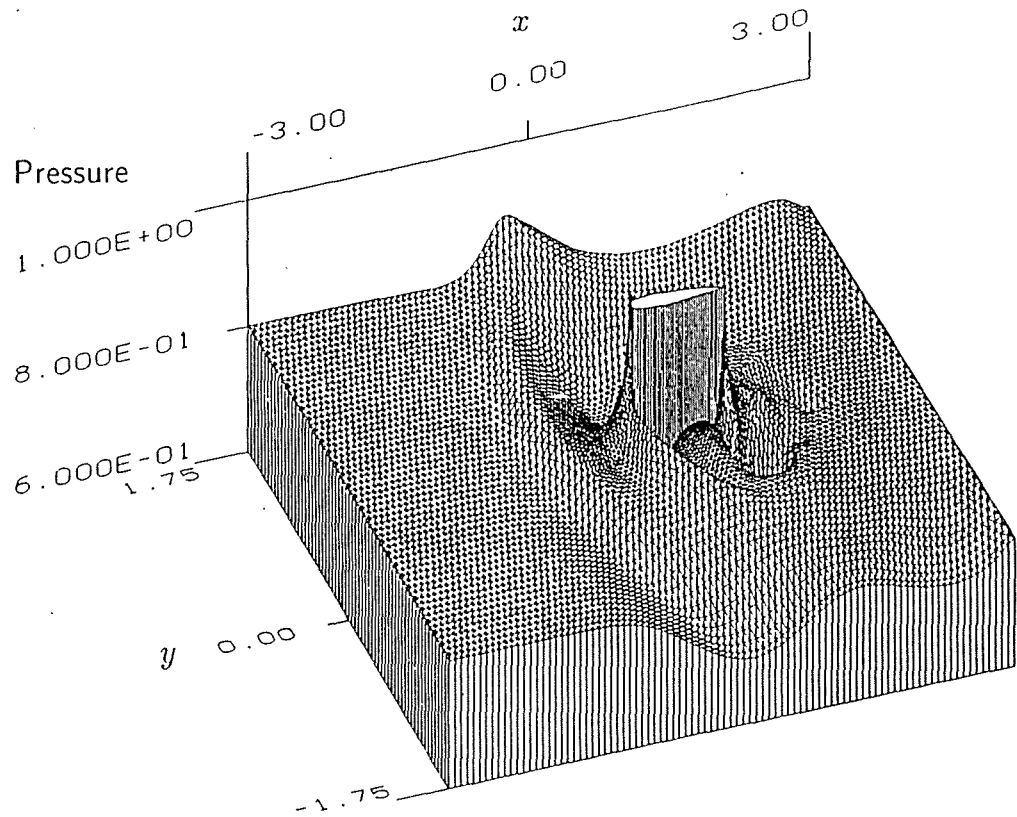


Fig. 4: Pressure distribution at $t = 4.8$, same as Fig. 3c

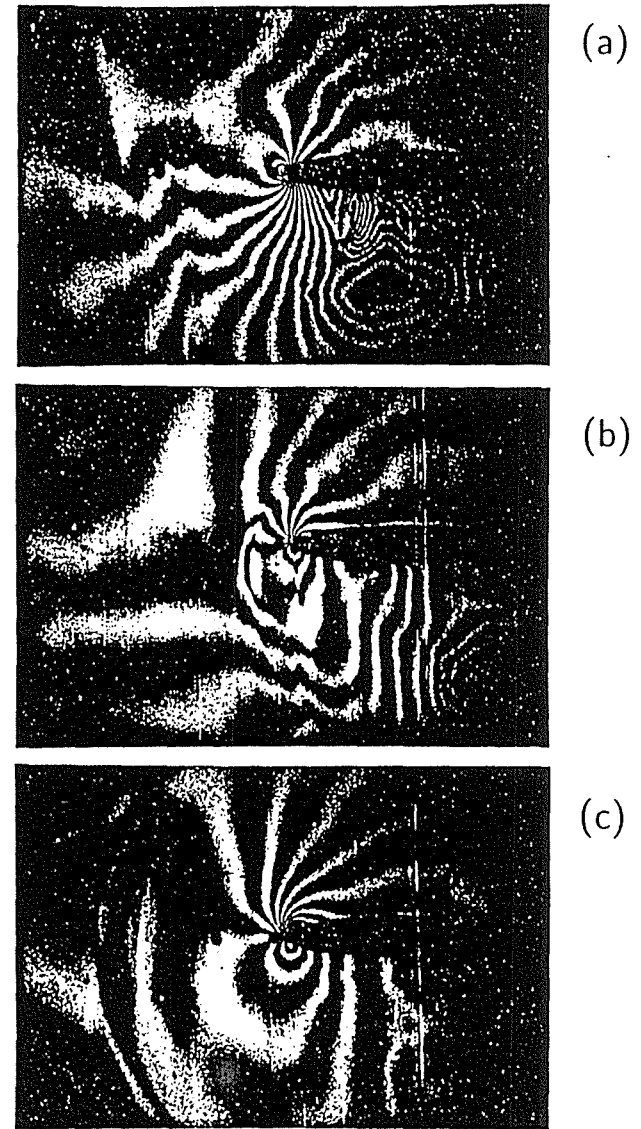


Fig. 5: Interferograms showing the generation of the *transonic wave*; OLS-profile, $Ma \approx 0.6$, time step = $0.2msec$,

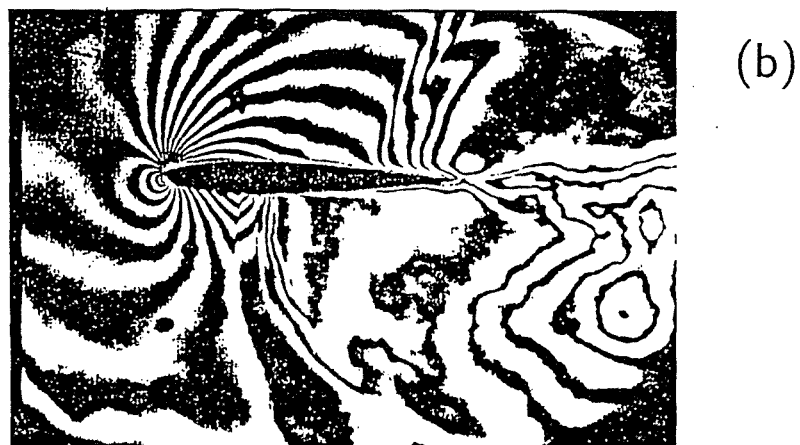
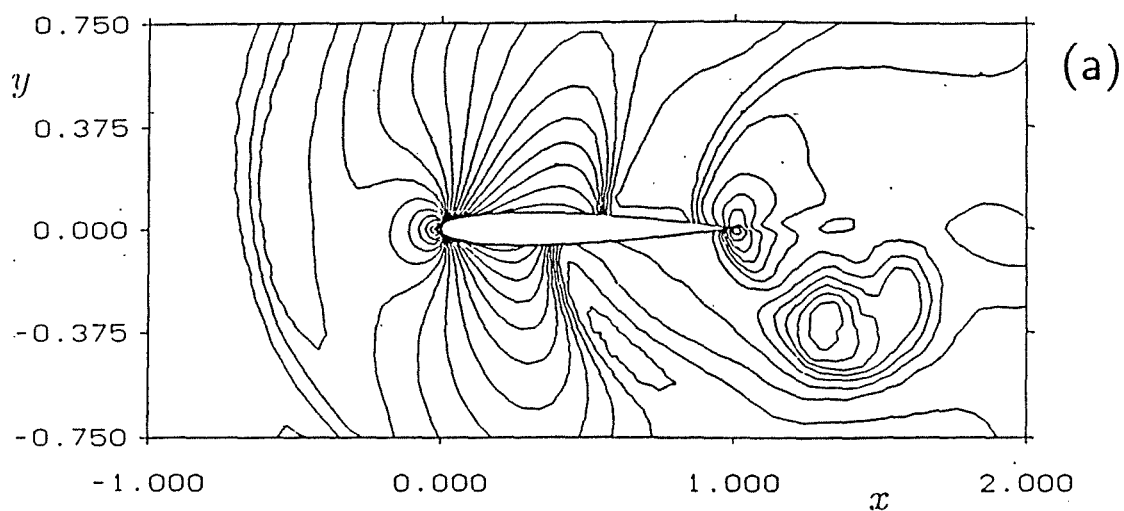


Fig. 6: Qualitative comparison of numerical with experimental density distribution; (a) Calculation: $Ma \approx 0.73$, $\bar{\Gamma}_{max} = 1.28$, $y_0 = -0.25$, $t = 4.0$; (b) Experiment: $Ma \approx 0.8$, $y_0 = -0.25$